RESEARCH ARTICLE SUMMARY

ULTRAFAST OPTICS

Generation of extreme-ultraviolet beams with time-varying orbital angular momentum

Laura Rego*†, Kevin M. Dorney*†, Nathan J. Brooks, Quynh L. Nguyen, Chen-Ting Liao, Julio San Román, David E. Couch, Allison Liu, Emilio Pisanty, Maciej Lewenstein, Luis Plaja, Henry C. Kapteyn, Margaret M. Murnane, Carlos Hernández-García

INTRODUCTION: Light beams carry both energy and momentum, which can exert a small but detectable pressure on objects they illuminate. In 1992, it was realized that light can also possess orbital angular momentum (OAM) when the spatial shape of the beam of light rotates (or twists) around its own axis. Although not visible to the naked eye, the presence of OAM can be revealed when the light beam interacts with matter. OAM beams are enabling new applications in optical communications, microscopy, quantum optics, and microparticle manipulation. To date, however, all OAM beams—also known as vortex beams—have been static; that is, the OAM does not vary in time. Here we introduce and experimentally validate a new property of light beams, manifested as a time-varying OAM along the light pulse; we term this property the self-torque of light.

RATIONALE: Although self-torque is found in diverse physical systems (e.g., electrodynamics and general relativity), to date it was not realized that light could possess such a property, where no external forces are involved. Self-torque is an inherent property of light, distinguished from the mechanical torque exerted on matter by static-OAM beams. Extreme-ultraviolet (EUV) self-torqued beams naturally arise when the extreme nonlinear process of high harmonic generation (HHG) is driven by two ultrafast laser pulses with different OAM and time delayed with respect to each other. HHG imprints a time-varying OAM along the EUV pulses, where all subsequent OAM components are physically present. In the future, this new class of dynamic-OAM beams could be used for manipulating the fastest magnetic, topological, molecular, and quantum excitations at the nanoscale.

RESULTS: Self-torqued beams are naturally produced by HHG, a process in which an ultrafast laser pulse is coherently upconverted into the EUV and x-ray regions of the spectrum. By driving the HHG process with two time-delayed, infrared vortex pulses possessing different OAM, ℓ_1 and ℓ_2, the generated high harmonics emerge as EUV beams with a self-torque, $\hbar\xi_q \simeq \hbar q(\ell_2 - \ell_1)/t_d$, that depends on the properties of the driving fields—that is, their OAM content and their relative time delay (t_d)—and on the harmonic order (q). Notably, the self-torque of light also manifests as a frequency chirp along their azimuthal coordinate, which enables its experimental characterization. This ultrafast, continuous, temporal OAM variation that spans from $q\ell_1$ to $q\ell_2$ is much smaller than the driving laser pulse duration and changes on femtosecond (10^{-15} s) and even subfemtosecond time scales for high values of self-torque. The presence of self-torque in the experimentally generated EUV beams is confirmed by measuring their azimuthal frequency chirp, which is controlled by adjusting the time delay between the driving pulses. In addition, if driven by few-cycle pulses, the large amount of frequency chirp results in a supercontinuum EUV spectrum.

ON OUR WEBSITE

Read the full article at http://dx.doi.org/10.1126/science.aaw9486

CONCLUSION: We have theoretically predicted and experimentally generated light beams with a new property that we call the self-torque of light, where the OAM content varies extremely rapidly in time, along the pulse itself. This inherent property of light opens additional routes for creating structured light beams. In addition, because the OAM value is changing on femtosecond time scales, at wavelengths much shorter than those of visible light, self-torqued HHG beams can be extraordinary tools for laser-matter manipulation on attosecond time and nanometer spatial scales. ■

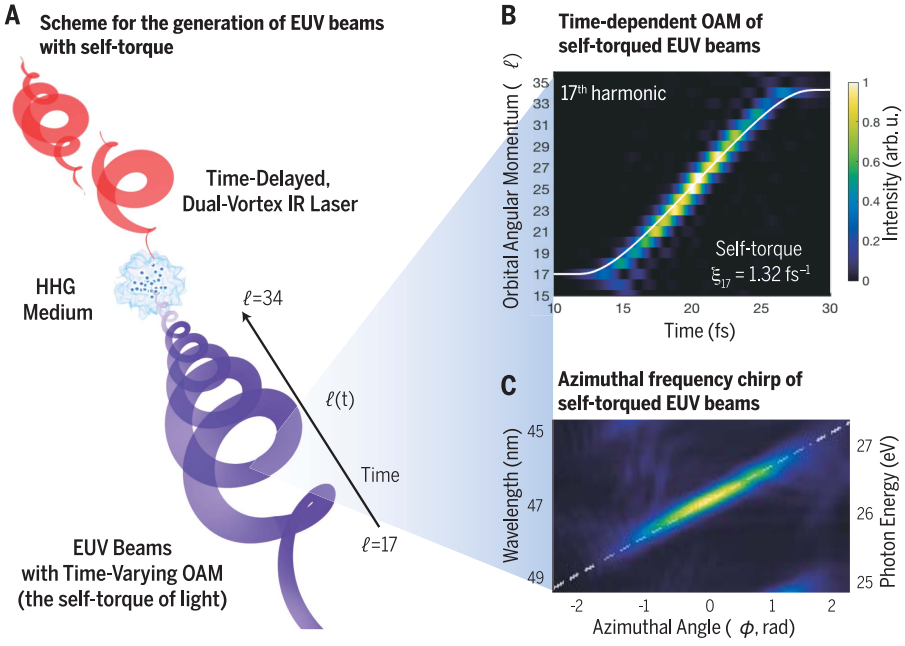

Generation of EUV beams with self-torque. (**A**) Two time-delayed, femtosecond infrared (IR) pulses with different OAM are focused into a gas target to produce self-torqued EUV beams through HHG. The distinctive signature of self-torqued beams is their time-dependent OAM, as shown in (**B**) for the 17th harmonic (47 nm, with self-torque ξ_{17} = 1.32 fs^{-1}). (**C**) The self-torque imprints an azimuthal frequency chirp, which enables its experimental measurement.

The list of author affiliations is available in the full article online.
*Corresponding author. Email: laura.rego@usal.es (L.R.); kevin.dorney@colorado.edu (K.M.D.)
†These authors contributed equally to this work.
Cite this article as L. Rego *et al.*, *Science* **364**, eaaw9486 (2019). DOI: 10.1126/science.aaw9486

RESEARCH ARTICLE

ULTRAFAST OPTICS

Generation of extreme-ultraviolet beams with time-varying orbital angular momentum

Laura Rego[1]*†, Kevin M. Dorney[2]*†, Nathan J. Brooks[2], Quynh L. Nguyen[2], Chen-Ting Liao[2], Julio San Román[1], David E. Couch[2], Allison Liu[2], Emilio Pisanty[3], Maciej Lewenstein[3,4], Luis Plaja[1], Henry C. Kapteyn[2,5], Margaret M. Murnane[2], Carlos Hernández-García[1]

Light fields carrying orbital angular momentum (OAM) provide powerful capabilities for applications in optical communications, microscopy, quantum optics, and microparticle manipulation. We introduce a property of light beams, manifested as a temporal OAM variation along a pulse: the self-torque of light. Although self-torque is found in diverse physical systems (i.e., electrodynamics and general relativity), it was not realized that light could possess such a property. We demonstrate that extreme-ultraviolet self-torqued beams arise in high-harmonic generation driven by time-delayed pulses with different OAM. We monitor the self-torque of extreme-ultraviolet beams through their azimuthal frequency chirp. This class of dynamic-OAM beams provides the ability for controlling magnetic, topological, and quantum excitations and for manipulating molecules and nanostructures on their natural time and length scales.

Structured light is critical for a host of applications in imaging and spectroscopy, as well as for enhancing our ability to optically manipulate macro- to nanoscale objects such as particles, molecules, atoms, and electrons. The distinctive phase and intensity properties of structured light beams achieved by exploiting the angular momentum of light have garnered renewed interest in optical manipulation and control (*1*). One of the most relevant structured light beams are those carrying orbital angular momentum (OAM), also known as vortex beams (*2*). The OAM of light manifests from a spatially dependent wavefront rotation of the light beam, which is characterized by the phase winding number, or topological charge, ℓ. OAM beams have been harnessed for applications in diverse fields (*3*) such as laser communication (*4*, *5*), phase-contrast (*6*, *7*) and superresolution microscopy (*8*), kinematic micromanipulation (*9*), quantum information (*10*), and lithography (*10*). Spurred by these exciting technologies, a paralleled interest in the ability to control and manipulate the OAM of ultrafast light pulses has also emerged, resulting in numerous techniques that can imprint OAM directly onto an arbitrary waveform. Diffractive and refractive optics (e.g., q-plates, spiral-phase plates, and holographic techniques) (*11*–*13*) can impart OAM onto waves from radio, to optical, and even x-ray (*14*) frequencies, and recent advances in high harmonic generation (HHG) have produced attosecond extreme-ultraviolet (EUV) pulses with designer OAM (*15*–*28*).

One of the most exciting capabilities enabled by OAM beams is their ability to exert photomechanical torques (*2*, *29*, *30*). Whereas the linear momentum of light can be employed to control and manipulate microscopic objects via the gradient and scattering forces associated with its intensity profile, optically induced torque manifests from angular momentum transfer between an object and a light field. This enables fundamental capabilities in advanced classical and quantum optical control and manipulation techniques, such as optical tweezers, lattices, and centrifuges (*9*, *31*–*34*), allowing for the realization of molecular and micromechanical rotors, single-particle trafficking, and fundamental studies of atomic motion in liquids and Bose-Einstein condensates (*35*, *36*).

We theoretically predict and experimentally validate the generation of light beams that carry time-dependent OAM, thus presenting a self-torque. This inherent property of structured light, the self-torque, $\hbar\xi$, is defined as $\hbar\xi = \hbar d\ell(t)/dt$, where $\hbar\ell(t)$ is the time-dependent OAM content of the light pulse. After being generated, the time-dependent OAM remains as a structural property of the light beam propagating in free space, where no interaction with external agents is present. Thus, the term self-torque refers to the inherent angular acceleration of the light beam, in an analogy with other physical systems that possess a self-induced time variation of the angular momentum—such as the radiation reaction of charged particles (*37*) or gravitational self-fields (*38*). Although OAM is well understood as a spatial property of light beams, to date, light pulses with time-dependent OAM have not been proposed or observed. We demonstrate that the self-torque arises as a necessary consequence of angular momentum conservation during the extreme nonlinear optical process of HHG. In HHG, the interaction of an intense field with an atom or molecule leads to the ionization of an electronic wave packet, which acquires energy from the laser field before being driven back to its parent ion, emitting a high-frequency photon upon recollision (*39*, *40*). The emitted harmonic radiation can extend from the EUV to the soft x-ray regime if the emissions from many atoms add together in phase (*41*–*44*). The resulting comb of fully coherent harmonics of the driving field in turn yields trains of phase-locked attosecond pulses (*45*, *46*).

Self-torqued light beams naturally emerge when HHG is driven by two time-delayed infrared (IR) pulses that differ by one unit of OAM (Fig. 1). The dynamical process of HHG makes it possible to imprint a continuous time-varying OAM, where all OAM components are present—thus creating self-torqued EUV beams. Intuitively, these exotic pulses can be understood as being composed of time-ordered photons carrying consecutively increasing OAM.

The self-torque of light translates to an azimuthal frequency chirp (i.e., a spectral shift along the azimuthal coordinate) on the radiation emission—and vice versa, which allows us to quantify the self-torque by an experimental measurement of the azimuthal frequency chirp. In addition, the degree of self-torque of EUV harmonic beams can be precisely controlled through the time delay and pulse duration of the driving, IR laser pulses. The generation of light beams with self-torque opens up a route for the investigation of systems with time-varying OAM that spontaneously appear in nature (*47*) as macroscopic dynamical vortices or—owing to the high frequency of the beams—microscopic ultrafast systems. For example, because short-wavelength light can capture the fastest dynamics in materials (*48*, *49*), self-torqued EUV beams can be expected to be used for imaging magnetic and topological excitations, launching selective and chiral excitation of quantum matter (*50*), imprinting OAM centrifuges (*32*), switching superpositions of adiabatic charge migration in aromatic or biological molecules (*51*, *52*), or manipulating the OAM dichroism of nanostructures (*53*) on attosecond time scales.

Theory underlying the self-torque of light

To create light beams with self-torque, we drive the HHG process with two linearly polarized IR

[1]Grupo de Investigación en Aplicaciones del Láser y Fotónica, Departamento de Física Aplicada, University of Salamanca, Salamanca E-37008, Spain. [2]JILA, Department of Physics, University of Colorado and NIST, Boulder, CO 80309, USA. [3]ICFO, Institut de Ciencies Fotoniques, The Barcelona Institute of Science and Technology, Av. Carl Friedrich Gauss 3, 08860 Castelldefels (Barcelona), Spain. [4]ICREA, Pg. Lluís Companys 23, 08010 Barcelona, Spain. [5]Kapteyn-Murnane Laboratories Inc. (KMLabs Inc.), 4775 Walnut Street no. 102, Boulder, CO 80301, USA.
***Corresponding author. Email: laura.rego@usal.es (L.R.); kevin.dorney@colorado.edu (K.M.D.)**
†These authors contributed equally to this work.

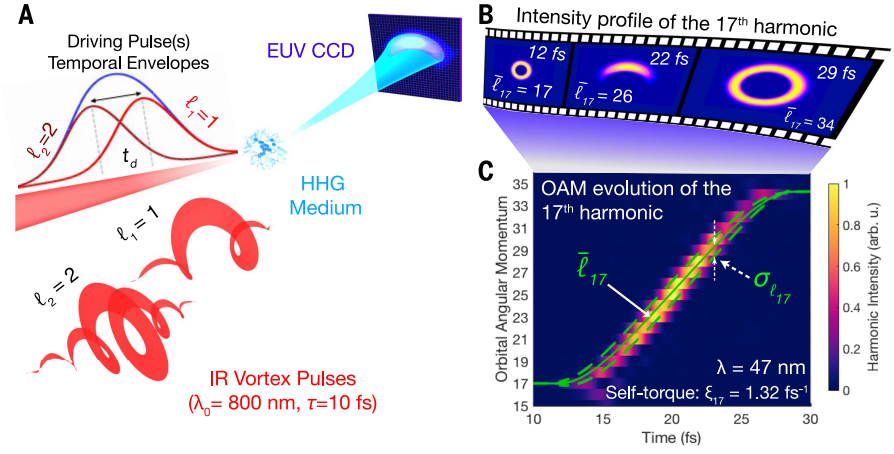

Fig. 1. Generation of EUV beams with self-torque. (**A**) Two time-delayed, collinear IR pulses with the same wavelength (800 nm), but different OAM values, are focused into an argon gas target (HHG medium) to produce harmonic beams with self-torque. The spatial profile of the complete, time-integrated, HHG beam from full quantum simulations is shown on the EUV CCD. (**B**) Predicted evolution of the intensity profile of the 17th harmonic at three instants in time during the emission process. (**C**) Temporal evolution of the OAM of the 17th harmonic, for two driving pulses with the same duration $\tau = 10$ fs, at a relative time delay of $t_d = \tau$. The average OAM, $\bar{\ell}_{17}$ (solid green), and the width of the OAM distribution, $\sigma_{\ell_{17}}$ (distance between the solid and dashed-green lines), are obtained from Eqs. 2 and 3. The self-torque associated with this pulse, $\xi_{17} = 1.32$ fs^{-1}, is obtained from the slope of the smooth and continuous time-dependent OAM.

pulses exhibiting the same frequency content (centered at $\omega_0 = 2\pi c/\lambda_0$), but with different OAM, ℓ_1 and ℓ_2, where $|\ell_1 - \ell_2| = 1$. The two laser pulses are separated by a variable time delay, t_d, which is on the order of the individual pulse widths (Fig. 1A) [see also supplementary text section S1 in (*54*)]. These two collinear IR vortex beams are then focused into an atomic gas target, such that the transverse intensity distribution of the two drivers exhibits maximum overlap. We model the HHG process using full quantum simulations in the strong-field approximation (SFA) that include propagation via the electromagnetic field propagator (*55*), a method that was used in several previous calculations of HHG involving structured pulses (*16*, *18*, *20*, *21*, *26*, *28*, *44*, *56*). We consider the driving vortex pulses possessing ℓ_1 and ℓ_2, described by a $\sin^2$ envelope with τ = 10 fs full width at half-maximum (FWHM) in intensity, centered at λ_0 = 800 nm, and delayed by $t_d = \tau$ = 10 fs (see materials and methods for further details). Figure 1A shows a schematic of the temporal envelopes of each pulse (red), as well as their superposition (blue). Figure 1C shows the time-dependent OAM of the 17th harmonic obtained from our simulations (color scale), whereas in Fig. 1B the spatial intensity distribution of the 17th harmonic is sketched at three instants of time during the emission process. To extract the temporal variation of the OAM, we first select the HHG spectrum in the frequency range $(q-1)\omega_0$ to $(q+1)\omega_0$ (where q is the harmonic order to explore, being q = 17 in Fig. 1), and then we perform a Fourier transform along the azimuthal coordinate (*20*) at each time instant along the harmonic pulse. Notably, the temporal variation of the OAM is monotonic and continuous, spanning over an entire octave of consecutive topological charges—i.e., it includes all OAM components from $q\ell_1 = 17$ to $q\ell_2 = 34$.

The nature of self-torqued beams can be understood through a simple theoretical analysis. Previous works in OAM-HHG have demonstrated that an IR vortex beam can be coherently converted into high-frequency vortex beams (*15*–*28*). When HHG is driven by a single, linearly polarized, IR vortex beam with integer topological charge, ℓ_1, the OAM of the qth-order harmonic follows a simple scaling rule, $\ell_q = q\ell_1$ (*16*, *17*). This scaling reflects the nature of OAM conservation in HHG, where q IR-photons combine to produce the qth-order harmonic. If HHG is driven by the combination of two collinear and temporally overlapped IR vortices with different OAM, ℓ_1 and ℓ_2, each harmonic order will span over a wide OAM spectrum, given by $\ell_q = n_1\ell_1 + n_2\ell_2$ (*20*), where n_1 and n_2 are the number of photons absorbed from each driver ($n_1 + n_2 = q$, whose total must be odd due to parity restrictions). Each channel, (n_1, n_2), is weighted according to a binomial distribution, associated with the different combinations of absorbing n_1 photons with ℓ_1 and n_2 photons with ℓ_2. The effect of the harmonic intrinsic phase in the OAM spectrum, also explored in (*20*), is second order, and negligible for the results presented here.

In this work, we consider the HHG fields that can be produced by two IR laser vortex pulses separated by some time delay. The superposition of the delayed envelopes turns into a temporal dependence in the relative weights of the driving fields—thus introducing time as an additional parameter. To show how this influences the OAM structure of the EUV harmonics, we consider two time-delayed, collinear, linearly polarized, IR driving pulses with different OAM, ℓ_1 and ℓ_2. We denote, in cylindrical coordinates (ρ, ϕ, z), the complex amplitudes of the driving fields at the focus position (z = 0) as $U_1(\rho, \phi, t)$ and $U_2(\rho, \phi, t)$. For simplicity, we consider the field amplitudes at the ring of maximum intensity at the target—where the HHG efficiency is highest—and the resulting field can be written as $U(\phi, t) = U_0(t)\{[1-\eta(t)]e^{i\ell_1\phi} + \eta(t)e^{i\ell_2\phi}\}$, where $U_0(t) = U_1(t) + U_2(t)$ and $\eta(t) = U_2(t)/U_0(t)$ is the relative amplitude of the second beam. According to the strong-field description of HHG, the amplitude of the qth-order harmonic, $A_q(\phi, t)$, scales nonperturbatively with that of the driving laser, with an exponent $p < q$ [$p \simeq 4$ for our laser parameters (*20*)], whereas the qth-order harmonic phase is considered to be q times that of the driver (see supplementary text section S1 for the complete derivation); thus

$$A_q(\phi, t) \propto U_0^p(t) \times \left[\sum_{r=0}^{p} \binom{p}{r} (1-\bar{\eta}(t))^r e^{ir\ell_1\phi} \bar{\eta}^{(p-r)}(t) e^{i(p-r)\ell_2\phi}\right] \times e^{i(q-p)[(1-\bar{\eta}(t))\ell_1 + \bar{\eta}(t)\ell_2]\phi} \quad (1)$$

where r is an integer and $\bar{\eta}(t)$ is the average of $\eta(t)$ over the time it takes the ionized electron to complete the rescattering trajectory that contributes to the generation of a particular harmonic. For this average, we have considered the so-called short trajectories (*57*, *58*), whose excursion time can be approximated to half a cycle. The contribution of long trajectories to the OAM content is two orders of magnitude weaker than that of the short ones (*20*). The summation in Eq. 1 is carried over p different OAM channels, each weighted by a binomial distribution in accordance with the combinatory nature of the HHG up-conversion process. Parity conservation in HHG demands that the total number of photons absorbed from each driving field, $n_1 + n_2$, must be odd, which implies that to generate all intermediate OAM states between $q\ell_1$ and $q\ell_2$, the OAM of the drivers must differ by one unit, i.e., $|\ell_1 - \ell_2|$ =1. The mean OAM of the qth-order harmonic at any instant of time along the harmonic pulse is given by [see (*54*)]

$$\bar{\ell}_q(t) = q\left[(1-\bar{\eta}(t))\ell_1 + \bar{\eta}(t)\ell_2\right] \quad (2)$$

and the width of the OAM distribution is

$$\sigma_{\ell_q} = |\ell_2 - \ell_1|\sqrt{p\bar{\eta}(t)\left(1-\bar{\eta}(t)\right)} \quad (3)$$

In analogy with mechanical systems, we characterize the time-varying OAM spectrum of the qth-order harmonic via the self-torque

$$\xi_q = d\bar{\ell}_q(t)/dt \quad (4)$$

As the OAM of light is defined as $\hbar\ell$, the self-torque is given by $\hbar\xi$. For simplicity we factor

out $\hbar$ and denote the self-torque by ξ, in units of fs^{-1}. It is worth mentioning that σ_{ℓ_q} depends weakly on the harmonic order, as the parameter p remains almost constant along the nonperturbative spectral plateau. The nonperturbative nature of the HHG process reduces the number of available channels to generate the qth-order harmonic from q (perturbative) to $p \sim 4$ (nonperturbative). As typically $p << q$, $\bar{\ell}_q(t)$ appears as a well-defined quantity whose relative error, $\sigma_{\ell_q}/\bar{\ell}_q$, decreases as the harmonic order increases. Thus, $\bar{\ell}_q(t)$ approaches the classical behavior, i.e., its relative uncertainty tends to 0 in the limit of large harmonic orders, converging to perfectly defined intermediate OAM states.

In Fig. 1C, we show the temporal evolution of the mean OAM of the 17th harmonic, $\bar{\ell}_{17}$ (solid-green line), and its OAM width, $\sigma_{\ell_{17}}$ (dashed-green lines). In this case, where $t_d = \tau$, we can approximate the self-torque as constant over the OAM span:

$$\xi_q \sim q(\ell_2 - \ell_1)/t_d \tag{5}$$

which provides a straightforward route for controlling the self-torque through the OAM of the driving pulses and their temporal properties. The example shown in Fig. 1C corresponds to a self-torque of $\xi_{17} = 1.32\ fs^{-1}$, which implies an attosecond variation of the OAM. Equation 5 is valid only if $t_d \simeq \tau$, and if this condition is relaxed, the self-torque must be calculated from the definition given by Eq. 4. Actually, $t_d = \tau$ is a particularly interesting case, as it corresponds to the time delay where the weight of all intermediate OAM states is more uniform over all the OAM span (see fig. S1 for the time-dependent OAM for different time delays, showing a consistently excellent agreement between the full quantum simulations and the OAM content predicted by Eqs. 2 and 3).

It is important to stress that even though the mean OAM value at each instant of time may be a noninteger, the nature of self-torqued beams is different from that of the well-known fractional OAM beams (*21*, *59*–*61*). In particular, the mere superposition of two time-delayed vortex beams—carrying $\ell_i = q\ell_1$ and $\ell_f = q\ell_2$ units of OAM, respectively—does not contain a self-torque. Although it does lead to a temporal variation of the average OAM similar to that in Eq. 2, it does not contain physical intermediate OAM states, i.e., photons with OAM other than ℓ_i and ℓ_f. Self-torqued beams, by contrast, contain all intermediate OAM states, which are time-ordered along the pulse (see Fig. 1C).

In addition, the width of the instantaneous OAM distribution of self-torqued beams (Eq. 3) is much narrower than that of the mere superposition of two time-delayed OAM beams—which in the case of $\ell_i = q\ \ell_1$ and $\ell_f = q\ \ell_2$ is $\sigma_{\ell_q} = q|\ell_2 - \ell_1|\ \sqrt{\eta(t)(1-\eta(t))}$. This is a result of the nonperturbative behavior of HHG, which enables the creation of well-defined intermediate OAM states in a self-torqued beam. In Movie 1 (and in figs. S3 and S4) we further evidence the distinctions in the temporal evolution of the OAM content and phase and intensity profiles between self-torqued beams and the mere superposition of two time-delayed OAM beams. In the latter case, the phase and intensity profiles remain q-fold symmetric, whereas in self-torqued beams, the q-fold symmetry is broken. This breakdown in rotational symmetry is manifested in both the intensity distribution and the corresponding phase profiles of the self-torqued beams. Whereas the intensity distribution exhibits a characteristic "crescent" shape due to the coherent combination of vortex beams with subsequent OAM charges ($\ell_i + \ell_{i+1}$, as previously shown in Fig. 1), the associated phase profiles show the continuous appearance of new vortex singularities along a single row. In other words, a self-torqued beam can be understood as a topological structure where new vortices emerge one at a time.

It is of paramount relevance to evidence the physical nature of the self-torqued beams by temporally characterizing the intermediate OAM states, $\ell_q(t_k)$, with $q\ell_1 < \ell_q(t_k) < q\ell_2$. Assuming a beam with constant self-toque ξ_q, the component of the qth-order harmonic carrying an OAM of $\ell_q(t_k)$ will appear at the time $t_k = \frac{\ell_q(t_k) - q\ell_1}{\xi_q}$ after the peak amplitude of the first driving pulse, exhibiting a temporal width, according to Eq. 3, of $\Delta t_k = \frac{\sigma_{\ell_q}}{\xi_q} = \tau\frac{\sqrt{p\bar{\eta}(1-\bar{\eta})}}{q} \ll \tau$. Therefore, a self-torqued pulse can be thought of as a pulse with a time-dependent OAM, with a temporal OAM variation much smaller than the width of the driving pulses, reaching the attosecond time scale for sufficiently high values of self-torques. This allows us to stress the difference between self-torqued beams and a train of nonoverlapping pulses with different OAM (*62*). Finally, in analogy to polarization gating techniques (*63*), self-torqued EUV beams open the possibility of subfemtosecond OAM-gating techniques, providing a high degree of temporal control over laser-matter interactions involving OAM.

The azimuthal frequency chirp of self-torqued beams

A direct consequence of self-torque is the presence of an azimuthal frequency chirp in the light beam. As the phase term associated with a time-dependent OAM is given by $\ell_q(t)\phi$, the instantaneous frequency of the qth-order harmonic—given by the temporal variation of the harmonic phase, $\varphi_q(t,\ \phi)$—is shifted by the self-torque as

$$\omega_q(t,\phi) = \frac{d\varphi_q(t,\phi)}{dt} = \omega_q + \frac{d\ell_q(t)}{dt}\phi \approx \omega_q + \xi_q\phi \tag{6}$$

Therefore, the harmonics experience an azimuthal frequency chirp whose slope is the self-torque. Although $\omega_q(t,\phi)$ in Eq. 6 is a continuous function of $\phi(-\pi \le \phi < \pi)$, the null intensity region in the crescent profile of the beam (see inset in Fig. 2A) avoids the frequency discontinuity. However, further studies on this region of "structured darkness" (*61*) could be beneficial for a thorough fundamental understanding of self-torqued beams.

We present in Fig. 2 the HHG spectrum along the azimuthal coordinate obtained in our full quantum simulations for driving pulses of $\tau = 10$ fs and time delays of (A) $t_d = \tau = 10$ fs and (B) $t_d = -\tau = -10$ fs, respectively. The intensity crescent shape of the whole HHG beam is shown in the inset of Fig. 2A. Both spectra reflect the presence of an azimuthal chirp that depends on the harmonic order, and thus, an associated self-torque, whose sign depends on t_d. The full quantum simulations are in perfect agreement with the analytical estimation given by Eq. 6 (gray

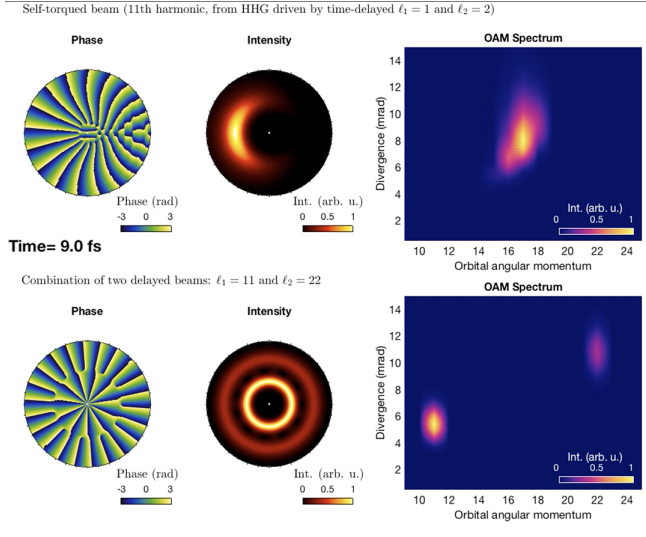

Movie 1. Comparison between the temporal evolution of phase, intensity, and OAM content of self-torqued beams and two delayed vortex beams. Temporal evolution of the phase (left column), intensity (central column), and OAM distribution along the divergence (right column) of a self-torqued beam (top) and a combination of two time-delayed vortex beams. The self-torqued beam (top) corresponds to the 11th harmonic generated through HHG ($\ell_1 = 1$, $\ell_2 = 2$, $\tau = 10$ fs, $t_d = 10$ fs, $\lambda_1 = \lambda_2 = 800$ nm) calculated using the thin slab model (see supplementary text section S2), whereas the vortex combination (bottom) corresponds to two time-delayed vortex beams ($\ell_1 = 11$, $\ell_2 = 22$, $\tau = 10$ fs, $t_d = 10$ fs, $\lambda_1 = \lambda_2 = 800$ nm).

dashed lines). This result shows that the spectral bandwidth of the harmonics can be precisely controlled via the temporal and OAM properties of the driving pulses. Moreover, it provides a direct, experimentally measurable parameter to extract the self-torque, without measuring the OAM of each harmonic at each instant of time with subfemtosecond resolution, which is currently unfeasible. This reasoning implies that a beam with azimuthal frequency chirp would also exhibit self-torque. Up to now, however, HHG beams have only been driven either by spatially chirped pulses [such as the so-called "attosecond lighthouse" technique (*64*, *65*)], or angularly chirped pulses through simultaneous spatial and temporal focusing, which (in theory) yield spatially chirped harmonics (*66*). However, to the best of our knowledge, azimuthal chirp—and thus, self-torque—has not been imprinted into EUV harmonics or in any other spectral regime.

Experimental confirmation of the self-torque of EUV beams

Light beams possessing a self-torque were experimentally generated by driving the HHG process in argon gas using two collinear, IR vortex beams with topological charges $\ell_1 = 1$ and $\ell_2 = 2$ that are derived from a high-power, ultrafast regenerative amplifier (Fig. 3A). Briefly (see materials and methods for full details), the two vortex beams are spatiotemporally overlapped to yield a mixed OAM driving mode, which is then directed onto a supersonic expansion of argon gas to generate self-torqued EUV beams (q = 13 to 23, ~20 to 36 eV). The presence of self-torque in the emitted high harmonics is confirmed by using a cylindrical mirror–flat-grating EUV spectrometer that serves to transform the self-torque-induced azimuthal chirp into a spatial chirp, which is then spectrally resolved as the (1D) focusing harmonic beam is dispersed (Fig. 3B). This simultaneous mapping of the azimuthal frequency chirp and high-harmonic comb to the same spectral axis is achieved by aligning the intensity crescent of the EUV beam [see materials and methods and (*54*)] such that its intensity-weighted center of mass (COM) is orthogonal to the mutually parallel focusing and dispersion axes of the EUV spectrometer. In this configuration, the azimuthal frequency chirp is mapped to a linear spatial chirp by the cylindrical mirror, and this resulting spatial chirp in each harmonic is then resolved by the grating. The resulting spatial-spectral distribution is then imaged via a high–pixel density, EUV charge-coupled device (CCD) camera, which allows for the simultaneous measurement of the azimuthal angular extent of the self-torqued beams (*54*) and the induced azimuthal frequency chirp with a high precision. High-resolution HHG spectra are collected as a function of time delay between the driving pulses by scanning the relative time delay between the two beams in two-cycle increments (i.e., 5.272 fs), which ensures that the HHG beam remains aligned to the spectrometer at each experimentally sampled time delay. Such exquisite control (fig. S6) allows us to simultaneously measure both the self-torque-induced frequency chirp of the HHG beams and the azimuthal angular range over a large range of relative time delays.

Figure 4 shows the comparison between experimental and theoretical results. Panels (A) and (B) show the experimental and theoretical spatial profile of the high harmonic beams, respectively. The crescent shape of the measured spatial profile already gives a clear indication of the presence of all intermediate OAM contributions from $q\ell_1$ to $q\ell_2$, and thus, of the creation of self-torqued beams. Panels (C) to (F) show

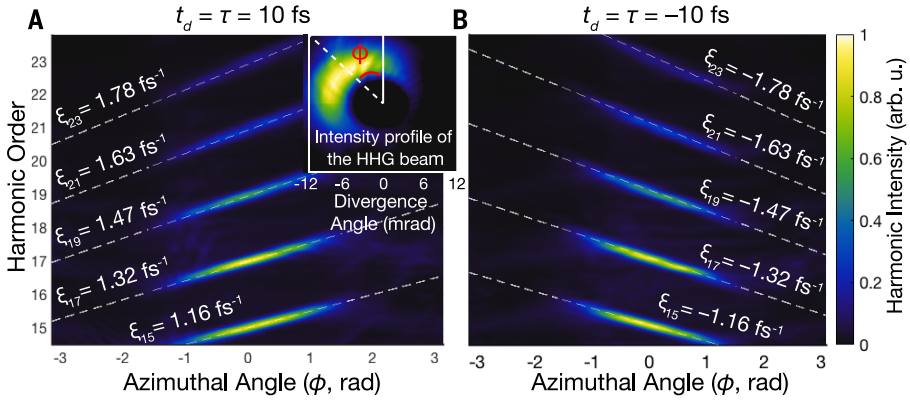

Fig. 2. Azimuthal frequency chirp of self-torqued beams. Simulated spatial HHG spectrum along the azimuthal coordinate (ϕ) when the time delay between the driving pulses is (**A**) 10 fs and (**B**) −10 fs. The self-torque of light imprints an azimuthal frequency chirp, which is different for each harmonic, as indicated by the gray dashed lines (obtained from Eq. 6). The azimuthal frequency chirp serves as a direct measurement of the self-torque of each harmonic beam. The inset of (A) shows the intensity profile of the HHG beam, as well as the definition of the azimuth, ϕ.

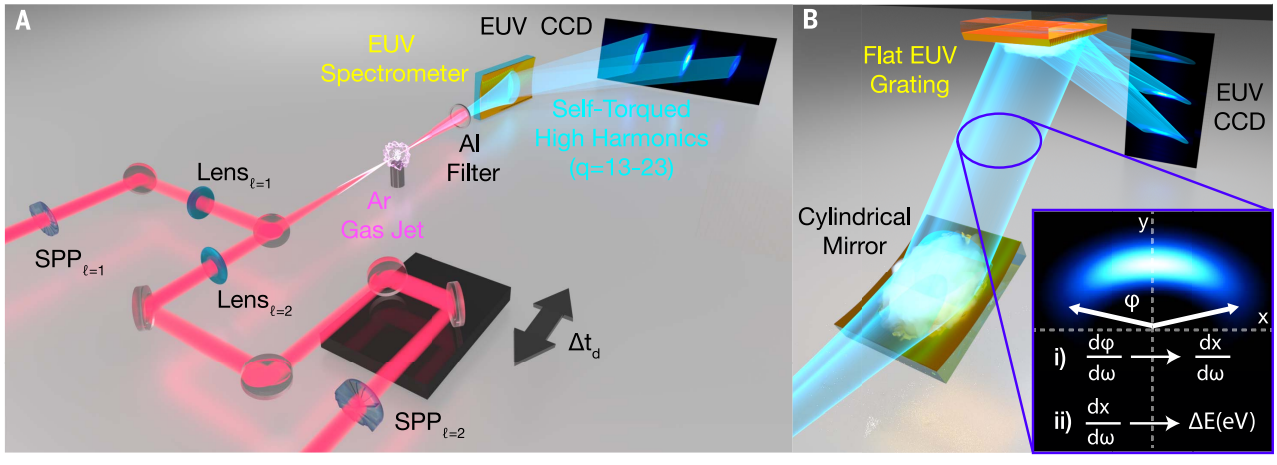

Fig. 3. Experimental scheme for generating and measuring light beams with a self-torque. (**A**) Two time-delayed, collinear IR pulses with the same wavelength (790 nm), but different OAM values, are focused into an argon gas target to produce harmonic beams with self-torque. (**B**) An EUV spectrometer, composed of a cylindrical mirror and flat-grating pair, collapses the HHG beam in the vertical dimension (lab frame y axis), while preserving spatial information, and thus the azimuthal extent in the transverse dimension (lab frame x axis). (Lower-right inset) The cylindrical mirror effectively maps the azimuthal frequency chirp into a spatial chirp along the lab frame x axis (i), which is then dispersed by the grating (ii).

the azimuthal chirp of the high harmonics for time delays of t_d = 50.4 (C and D) and −50.4 fs (E and F), respectively. The different slope of the azimuthal chirp, and the excellent agreement with the analytical theory given by Eq. 6 (gray dashed lines), and the full quantum simulations, confirm the presence of self-torque in the retrieved harmonic beams. Driving pulses of $\tau = 52$ fs have been used in our full quantum simulations to mimic the experimental parameters.

In Fig. 5, we plot the experimental (solid lines) and theoretical (dashed lines) self-torques obtained for the 17th (A), 19th (B), 21st (C), and 23rd (D) harmonics as a function of the time delay between the IR drivers, for the same parameters as in Fig. 4. As the time delay is varied, so too is the degree of azimuthal frequency chirp across the entire harmonic spectrum (according to Eqs. 2 and 6), verifying the dynamical build-up of OAM in the self-torqued beams. The self-torque is extracted from the measured azimuthal spectral shift (see Fig. 4F) and the azimuthal extent of the HHG beam [see (*54*) for details], using Eq. 6. The excellent agreement and, especially, the overall trend, unequivocally demonstrate the presence of a temporally evolving OAM content and, thus, a self-torque, in all the EUV harmonics generated.

Self-torque versus time duration and EUV supercontinuum generation

EUV beams with self-torque can be generated and controlled via the properties of the driving IR vortex beams, with optimal self-torque produced when the laser pulse separation is equal to their duration (i.e., $t_d = \tau$), where all intermediate OAM contributions appear with a similar weight (fig. S1). To illustrate this concept, Fig. 6A shows the simulated self-torque obtained for different IR driving pulse durations.

In particular, if driven by few-cycle pulses, the self-torque—and thus the azimuthal chirp—is high, with large amounts of OAM building up on an attosecond time scale (Fig. 6B, where $\tau = 4$ fs). If the torque is high enough, the harmonic frequency comb sweeps along the azimuth, encapsulating all the intermediate frequencies between the teeth of the harmonic comb. Thus, the frequency chirp of time-dependent OAM beams not only is useful to measure the self-torque but also represents an approach to obtain an EUV supercontinuum, as shown in the right inset of Fig. 6B. This allows for the creation of a very precise, azimuthally tunable frequency comb in the EUV and a supercontinuum spectrum that is complementary, yet distinct, from that of other approaches (*67*–*69*).

Conclusions

We have demonstrated that light beams with time-dependent OAM can be created, thus carrying optical self-torque. This property spans the applications of structured light beams (*1*) by adding a new degree of freedom, the self-torque, and thus introducing a new route to control light-matter interactions. In particular, ultrafast, short-wavelength, high harmonic beams with

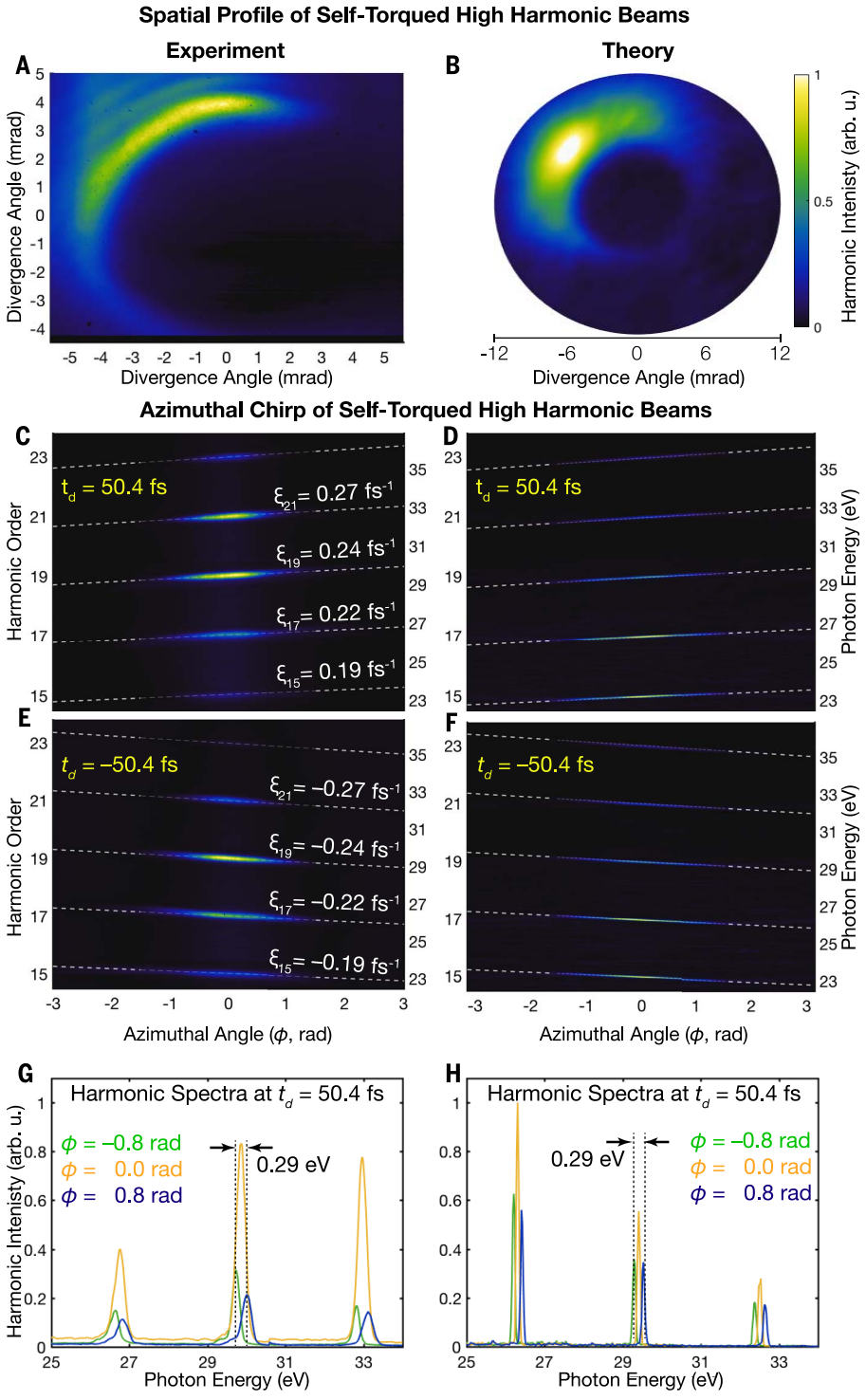

Fig. 4. Azimuthal frequency chirp and experimental measurement of the self-torque of EUV beams. (**A** and **B**) Experimental and theoretical spatial intensities of the HHG beams, after passing through an Al filter, comprising harmonics q = 13 to 23. (**C** to **F**) Spatial HHG spectrum along the azimuthal coordinate (ϕ) from experiment [(C) and (E)] and quantum simulations [(D) and (F)], when the time delay between the driving pulses is [(C) and (D)] 50.4 fs and [(E) and (F)] −50.4 fs. The self-torque of light imprints an azimuthal frequency chirp, which is different for each harmonic, as indicated by the gray dashed lines (obtained from Eq. 6). (**G** and **H**) Theoretical and experimental harmonic lineouts obtained at ϕ = −0.8 rad (green), ϕ = 0.0 rad (yellow), and ϕ = 0.8 rad (blue) for t_d= 50.4 fs. The azimuthal frequency chirp serves as a direct measurement of the self-torque of each harmonic beam. Differences in mode size of the theoretical and experimental EUV beam are due to slight differences in the fundamental beam mode sizes (see materials and methods).

self-torque can be naturally produced by taking advantage of the conservation laws inherent to extreme nonlinear optics. This capability can yield distinctively structured light beams that can deliver optical torque on the natural time and length scales of charge and spin ordering, e.g., femtosecond and nanometer. Finally, the self-torque of light imprints an azimuthal frequency chirp, which allows a way to experimentally measure and control it. Moreover, if the self-torque is high enough, the harmonic frequency comb sweeps smoothly along the azimuth, and if integrated, a high-frequency supercontinuum is obtained, thus presenting exciting perspectives in EUV and ultrafast spectroscopies of angular momentum dynamics.

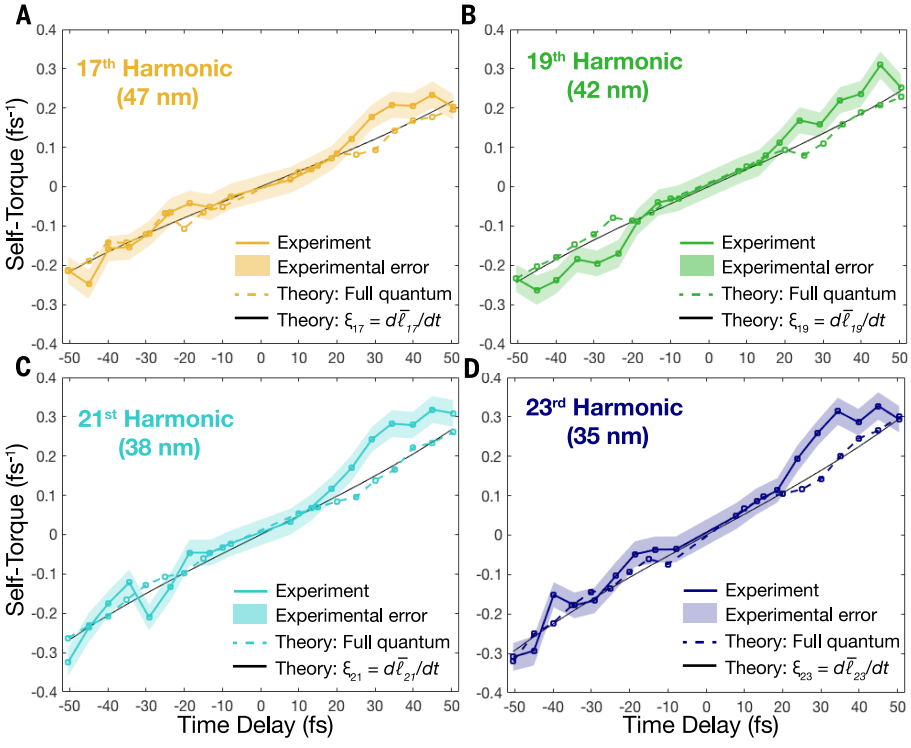

Fig. 5. Experimental confirmation of the self-torque of light in EUV beams. Self-torques obtained as a function of the time delay between the IR laser drivers for the 17th (**A**), 19th (**B**), 21st (**C**), and 23rd (**D**) harmonics. The experimental data are shown in solid-color lines, the results from full quantum simulations in dashed lines, and the analytical estimation given by Eq. 2 in solid black lines. The shaded regions depict the experimental uncertainty in the retrieved self-torque for each harmonic order, which themselves comprise the standard "one sigma" deviation of the measured self-torque (i.e., 68% of the measured self-torque values will fall within this uncertainty range).

Materials and methods

Theoretical approach for full quantum simulations describing the self-torque of OAM high harmonic beams

To calculate the HHG driven by two time-delayed OAM pulses, we use a theoretical method that computes both the full quantum single-atom HHG response and subsequent propagation (*55*). The propagation is based on the electromagnetic field propagator, in which we discretize the target (gas jet) into elementary radiators (*55*). The dipole acceleration of each elementary source is computed using the full quantum SFA, instead of solving directly the time-dependent Schrödinger equation, yielding a performance gain in computational time when computing HHG over the entire target (*55*). At the microscopic single-atom level, and for the parameters considered in this work, the spatial phase of the electric field can be well approximated as homogeneous in the vicinity of the atom where the wave packet dynamics take place. We assume that the harmonic radiation propagates with the vacuum phase velocity, which is a reasonable assumption for high-order harmonics. Propagation effects in the fundamental field, such as the production of free charges, the refractive index of the neutrals, and the group velocity walk-off, as well as absorption in the propagation of the harmonics, are taken into account. Although we account for the time-dependent nonlinear phase shifts in the driving fields, nonlinear spatial effects are not taken into account. We consider two vortex beams with $\ell_1 = 1$ and $\ell_2 = 2$, whose spatial structure is represented by a Laguerre-Gaussian beam [see

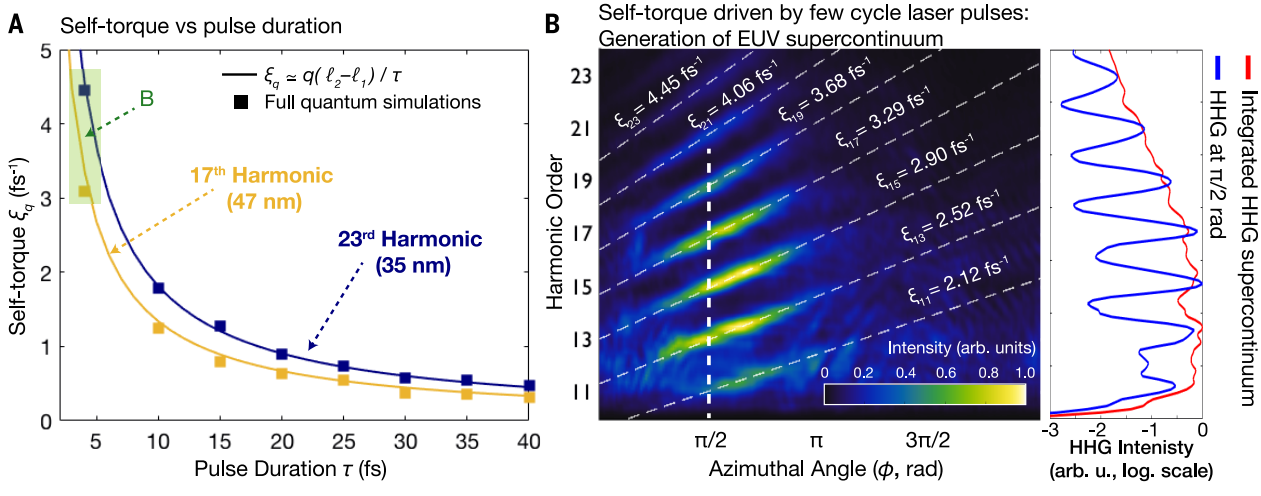

Fig. 6. Manifestation of self-torque for EUV supercontinuum generation. (**A**) Self-torque as a function of pulse duration for the 17th and 23rd harmonics, for time delays equal to their pulse duration. Solid lines are calculated from Eq. 2, and the squares correspond to results from full quantum simulations. (**B**) Spatiospectral HHG distributions when driven by two 800-nm, 4-fs pulses with ℓ_1=1 and ℓ_2=2, delayed by 4 fs with respect to each other. The optical self-torque imprints an azimuthal frequency chirp, which is different for each harmonic order, as indicated by the gray dashed lines (obtained from Eqs. 5 and 6). The right panel shows the HHG yield at $\pi/2$ rad (blue line, and white vertical dashed line in B) and the spatially integrated supercontinuum (red line).

eq. S13 in (*54*)]. The laser pulses are modeled with a $\sin^2$ envelope whose FWHM in intensity is τ, and centered at 800 nm in wavelength. The amplitudes of the two fields are chosen to obtain the same peak intensity (1.4×10^{14} W/cm^2) at focus for each driver at the radii of maximum superposition (i.e., the brightest intensity rings overlap spatially). The driving beam waists are chosen to overlap at the focal plane (being $w_1 = 30.0\,\mu$m for ℓ_1, and $w_2 = w_1/\sqrt{2} = 21.4\,\mu$m for ℓ_2) where a 10-μm-wide Ar gas jet flows along the direction perpendicular to the beam propagation, with a peak pressure of 667 Pa (5 torr). The low thickness of the gas jet is due to computational time limitations; however, on the basis of our previous results of OAM-HHG (*18*), we do not foresee any fundamental deviation when considering thicker gas jets closer to the experimental jet used in this work (a diameter of 150 μm).

Experimental setup for the generation and characterization of self-torqued EUV beams

The generation of self-torqued high-harmonics is achieved by impinging a pair of collinear, linearly polarized, nondegenerate IR-vortex beams onto a supersonic expansion of argon gas. The IR vortex beams (with topological charges of $\ell_1 = 1, \ell_2 = 2$) are derived from a high-power, ultrafast regenerative amplifier (790 nm, 40 fs, 9 mJ, 1 kHz, KMLabs Wyvern HE). The near full output of the amplifier is sent into a frequency-degenerate Mach-Zehndertype interferometer, which separates and later recombines the two driving pulses to form the dual-vortex IR driver. In each spatially separated arm of the interferometer, a combination of half-waveplates, faceted spiral phase plates (16 steps per phase ramp, HoloOr), and independent focusing lenses result in each beam possessing linear polarization, nondegenerate topological charges, and similarly sized intensity rings at focus. Independent irises in each beam path allow for fine tuning of the transverse mode size at focus and are used to match the size of the maximum-intensity ring for each driver. Using this strategy, the two driving beams possessed a full diameter of the intensity of ~65 μm—corresponding to waists sizes of $w_{\ell_1} \approx 45\,\mu$m and $w_{\ell_2} \approx 33\,\mu$m (*70*). The driving laser modes themselves, both individually and combined, are characterized by a modified Gerchberg-Saxton phase retrieval algorithm, which solves for the phase of a propagating light beam and allows extraction of the OAM content of the IR vortices (see supplementary text section S4), thus ensuring high-quality vortex beams for driving the HHG process (movie S1). This modified Gerchberg-Saxton method acquires and retrieves OAM content much faster than our previous characterization method using ptychography (*71*), but it is limited to nonmultiplexed (i.e., single-color) beams. A high-precision, high-accuracy, and high-repeatability delay stage (Newport, XMS-160S) is used to control the relative time delay between the two driving pulses, with subfemtosecond precision. The pulses are recombined at the output of the interferometer using a low-dispersion beam-splitter and then directed onto the supersonic expansion of argon gas in a vacuum chamber. We take extreme care to ensure that the two arms experience similar dispersion by using the same thickness and design of optics in each arm of the interferometer, which helps to reduce effects from carrier-to-envelope phase variation in the separate beam paths, while also ensuring similar pulse widths. Finally, the use of a frequency-degenerate Mach-Zehnder interferometer results in a 50% intensity loss of each driver when combined at the interferometer's exit; however, this configuration proved ideal to minimize pulse dispersion, while also allowing for independent control of the polarization and topological charge of the driving beams.

Self-torqued high harmonics are generated via the HHG up-conversion process, then dispersed in 1D via a cylindrical mirror–flat-grating EUV spectrometer and finally collected by a CCD camera (Andor Newton 940). A 200-nm-thick aluminum filter blocks the residual driving light before entering the spectrometer—while passing harmonics over its transmission range, ~17 to 72 eV—and all harmonic spectra are corrected for the transmission of the EUV beamline. To align the resulting HHG crescent to the spectrometer, we exploit the natural physics of time-delayed OAM beams. When two vortex beams with $\ell_1 = 1$ and $\ell_2 = 2$ are superposed, such that their amplitudes and intensity rings are equal, the resulting intensity distribution exhibits a characteristic crescent shape. The azimuthal orientation of the COM of the intensity crescent can be controlled via a relative phase delay between the two single-mode OAM drivers, such that a full-cycle phase delay (i.e., 2.635 fs for the 790-nm pulses used here) returns the intensity crescent to its initial position. By carefully adjusting the time delay between the two single-mode IR vortex beams, we can control the alignment of the intensity crescent of the driving beam [see (*54*)], and so to the resulting crescent-shaped harmonic beam (because, to first order, the HHG beam profile mimics the intensity distribution of the driving beam). Once the harmonic beam is aligned to the spectrometer, the relative phase delay between the driving beams is scanned in two-cycle increments (i.e., 5.272 fs), which ensures that the HHG beam remains aligned to the spectrometer at each experimentally sampled time delay. Such exquisite control (see fig. S6) allows us to simultaneously measure both the self-torque-induced frequency chirp of the HHG beam and the azimuthal angular range (see supplementary text section S7) with a high resolution.

REFERENCES AND NOTES

1. H. Rubinsztein-Dunlop *et al*., Roadmap on structured light. *J. Opt.* **19**, 013001 (2017). doi: 10.1088/2040-8978/19/1/013001
2. L. Allen, M. W. Beijersbergen, R. J. C. Spreeuw, J. P. Woerdman, Orbital angular momentum of light and the transformation of Laguerre-Gaussian laser modes. *Phys. Rev. A* **45**, 8185–8189 (1992). doi: 10.1103/PhysRevA.45.8185; pmid: 9906912
3. A. M. Yao, M. J. Padgett, Orbital angular momentum: Origins, behavior and applications. *Adv. Opt. Photonics* **3**, 161–204 (2011). doi: 10.1364/AOP.3.000161
4. A. E. Willner *et al*., Optical communication using orbital angular momentum beams. *Adv. Opt. Photonics* **7**, 66–106 (2015). doi: 10.1364/AOP.7.000066
5. A. Trichili *et al*., Optical communication beyond orbital angular momentum. *Sci. Rep.* **6**, 27674 (2016). doi: 10.1038/srep27674; pmid: 27283799
6. S. Fürhapter, A. Jesacher, S. Bernet, M. Ritsch-Marte, Spiral phase contrast imaging in microscopy. *Opt. Express* **13**, 689–694 (2005). doi: 10.1364/OPEX.13.000689; pmid: 19494929
7. M. A. Lauterbach, M. Guillon, A. Soltani, V. Emiliani, STED microscope with spiral phase contrast. *Sci. Rep.* **3**, 2050 (2013). doi: 10.1038/srep02050; pmid: 23787399
8. G. Vicidomini, P. Bianchini, A. Diaspro, STED super-resolved microscopy. *Nat. Methods* **15**, 173–182 (2018). doi: 10.1038/nmeth.4593; pmid: 29377014
9. M. Padgett, R. Bowman, Tweezers with a twist. *Nat. Photonics* **5**, 343–348 (2011). doi: 10.1038/nphoton.2011.81
10. J. P. Torres, L. Torner, *Twisted Photons: Applications of Light with Orbital Angular Momentum*. (Bristol: Wiley-VCH, 2011).
11. L. Marrucci, C. Manzo, D. Paparo, Optical spin-to-orbital angular momentum conversion in inhomogeneous anisotropic media. *Phys. Rev. Lett.* **96**, 163905 (2006). doi: 10.1103/PhysRevLett.96.163905; pmid: 16712234
12. M. W. Beijersbergen, R. P. C. Coerwinkel, M. Kristensen, J. P. Woerdman, Helical-wavefront laser beams produced with a spiral phase plate. *Opt. Commun.* **112**, 321–327 (1994). doi: 10.1016/0030-4018(94)90638-6
13. J. Atencia, M.-V. Collados, M. Quintanilla, J. Marín-Sáez, Í. J. Sola, Holographic optical element to generate achromatic vortices. *Opt. Express* **21**, 21056–21061 (2013). doi: 10.1364/OE.21.021056; pmid: 24103978
14. J. C. T. Lee, S. J. Alexander, S. D. Kevan, S. Roy, B. J. McMorran, Laguerre-Gauss and Hermite-Gauss soft x-ray states generated using diffractive optics. *Nat. Photonics* **13**, 205–209 (2019). doi: 10.1038/s41566-018-0328-8
15. M. Zürch, C. Kern, P. Hansinger, A. Dreischuh, C. Spielmann, Strong-field physics with singular light beams. *Nat. Phys.* **8**, 743–746 (2012). doi: 10.1038/nphys2397
16. C. Hernández-García, A. Picón, J. San Román, L. Plaja, Attosecond extreme ultraviolet vortices from high-order harmonic generation. *Phys. Rev. Lett.* **111**, 083602 (2013). doi: 10.1103/PhysRevLett.111.083602; pmid: 24010438
17. G. Gariepy *et al*., Creating high-harmonic beams with controlled orbital angular momentum. *Phys. Rev. Lett.* **113**, 153901 (2014). doi: 10.1103/PhysRevLett.113.153901; pmid: 25375710
18. C. Hernández-García, J. San Román, L. Plaja, A. Picón, Quantum-path signatures in attosecond helical beams driven by optical vortices. *New J. Phys.* **17**, 093029 (2015). doi: 10.1088/1367-2630/17/9/093029
19. R. Géneaux *et al*., Synthesis and characterization of attosecond light vortices in the extreme ultraviolet. *Nat. Commun.* **7**, 12583 (2016). doi: 10.1038/ncomms12583; pmid: 27573787
20. L. Rego, J. San Román, A. Picón, L. Plaja, C. Hernández-García, Nonperturbative twist in the generation of extreme-ultraviolet vortex beams. *Phys. Rev. Lett.* **117**, 163202 (2016). doi: 10.1103/PhysRevLett.117.163202; pmid: 27792355
21. A. Turpin, L. Rego, A. Picón, J. San Román, C. Hernández-García, Extreme ultraviolet fractional orbital angular momentum beams from high harmonic generation. *Sci. Rep.* **7**, 43888 (2017). doi: 10.1038/srep43888; pmid: 28281655
22. F. Kong *et al*., Controlling the orbital angular momentum of high harmonic vortices. *Nat. Commun.* **8**, 14970 (2017). doi: 10.1038/ncomms14970; pmid: 28378823
23. D. Gauthier *et al*., Tunable orbital angular momentum in high-harmonic generation. *Nat. Commun.* **8**, 14971 (2017). doi: 10.1038/ncomms14971; pmid: 28378741
24. C. Hernández-García, A twist in coherent X-rays. *Nat. Phys.* **13**, 327–329 (2017). doi: 10.1038/nphys4088
25. R. Géneaux *et al*., Radial index of Laguerre-Gaussian modes in high-order-harmonic generation. *Phys. Rev. A* **95**, 051801 (2017). doi: 10.1103/PhysRevA.95.051801
26. K. M. Dorney *et al*., Controlling the polarization and vortex charge of attosecond high-harmonic beams via simultaneous spin-orbit momentum conservation. *Nat. Photonics* **13**, 123–130 (2019). doi: 10.1038/s41566-018-0304-3
27. W. Paufler, B. Böning, S. Fritzsche, Tailored orbital angular momentum in high-order harmonic generation with bicircular Laguerre-Gaussian beams. *Phys. Rev. A* **98**, 011401 (2018). doi: 10.1103/PhysRevA.98.011401
28. E. Pisanty *et al*., Conservation of torus-knot angular momentum in high-order harmonic generation. *Phys. Rev. Lett.*

122, 203201 (2019). doi: 10.1103/PhysRevLett.122.203201; pmid: 31172784
29. M. Babiker, W. L. Power, L. Allen, Light-induced torque on moving atoms. *Phys. Rev. Lett.* **73**, 1239–1242 (1994). doi: 10.1103/PhysRevLett.73.1239; pmid: 10057660
30. H. He, M. E. Friese, N. R. Heckenberg, H. Rubinsztein-Dunlop, Direct observation of transfer of angular momentum to absorptive particles from a laser beam with a phase singularity. *Phys. Rev. Lett.* **75**, 826–829 (1995). doi: 10.1103/PhysRevLett.75.826; pmid: 10060128
31. A. T. O'Neil, M. J. Padgett, Three-dimensional optical confinement of micron-sized metal particles and the decoupling of the spin and orbital angular momentum within an optical spanner. *Opt. Commun.* **185**, 139–143 (2000). doi: 10.1016/S0030-4018(00)00989-5
32. D. M. Villeneuve *et al*., Forced molecular rotation in an optical centrifuge. *Phys. Rev. Lett.* **85**, 542–545 (2000). doi: 10.1103/PhysRevLett.85.542; pmid: 10991335
33. D. G. Grier, A revolution in optical manipulation. *Nature* **424**, 810–816 (2003). pmid: 12917694
34. M. E. J. Friese, H. Rubinsztein-Dunlop, J. Gold, P. Hagberg, D. Hanstorp, Optically driven micromachine elements. *Appl. Phys. Lett.* **78**, 547–549 (2001). doi: 10.1063/1.1339995
35. E. M. Wright, J. Arlt, K. Dholakia, Toroidal optical dipole traps for atomic Bose-Einstein condensates using Laguerre-Gaussian beams. *Phys. Rev. A* **63**, 013608 (2000). doi: 10.1103/PhysRevA.63.013608
36. A. Turpin *et al*., Blue-detuned optical ring trap for Bose-Einstein condensates based on conical refraction. *Opt. Express* **23**, 1638–1650 (2015). doi: 10.1364/OE.23.001638; pmid: 25835921
37. A. F. Rañada, L. Vázquez, On the self-torque on an extended classical charged particle. *J. Phys. Math. Gen.* **17**, 2011–2016 (1984). doi: 10.1088/0305-4470/17/10/013
38. S. R. Dolan *et al*., Gravitational self-torque and spin precession in compact binaries. *Phys. Rev. D Part. Fields Gravit. Cosmol.* **89**, 064011 (2014). doi: 10.1103/PhysRevD.89.064011
39. K. J. Schafer, B. Yang, L. F. DiMauro, K. C. Kulander, Above threshold ionization beyond the high harmonic cutoff. *Phys. Rev. Lett.* **70**, 1599–1602 (1993). doi: 10.1103/PhysRevLett.70.1599; pmid: 10053336
40. P. B. Corkum, Plasma perspective on strong field multiphoton ionization. *Phys. Rev. Lett.* **71**, 1994–1997 (1993). doi: 10.1103/PhysRevLett.71.1994; pmid: 10054556
41. A. Rundquist *et al*., Phase-matched generation of coherent soft x-rays. *Science* **280**, 1412–1415 (1998). doi: 10.1126/science.280.5368.1412; pmid: 9603725
42. R. A. Bartels *et al*., Generation of spatially coherent light at extreme ultraviolet wavelengths. *Science* **297**, 376–378 (2002). doi: 10.1126/science.1071718; pmid: 12130779
43. T. Popmintchev *et al*., Bright coherent ultrahigh harmonics in the keV x-ray regime from mid-infrared femtosecond lasers. *Science* **336**, 1287–1291 (2012). doi: 10.1126/science.1218497; pmid: 22679093
44. T. Fan *et al*., Bright circularly polarized soft X-ray high harmonics for X-ray magnetic circular dichroism. *Proc. Natl. Acad. Sci. U.S.A.* **112**, 14206–14211 (2015). doi: 10.1073/pnas.1519666112; pmid: 26534992
45. P. M. Paul *et al*., Observation of a train of attosecond pulses from high harmonic generation. *Science* **292**, 1689–1692 (2001). doi: 10.1126/science.1059413; pmid: 11387467
46. M. Hentschel *et al*., Attosecond metrology. *Nature* **414**, 509–513 (2001). doi: 10.1038/35107000; pmid: 11734845
47. B. Rodenburg *et al*., Influence of atmospheric turbulence on states of light carrying orbital angular momentum. *Opt. Lett.* **37**, 3735–3737 (2012). doi: 10.1364/OL.37.003735; pmid: 22941007
48. C. Chen *et al*., Distinguishing attosecond electron-electron scattering and screening in transition metals. *Proc. Natl. Acad. Sci. U.S.A.* **114**, E5300–E5307 (2017). doi: 10.1073/pnas.1706466114; pmid: 28630331
49. P. Tengdin *et al*., Critical behavior within 20 fs drives the out-of-equilibrium laser-induced magnetic phase transition in nickel. *Sci. Adv.* **4**, eaap9744 (2018). doi: 10.1126/sciadv.aap9744; pmid: 29511738
50. A. Picón *et al*., Transferring orbital and spin angular momenta of light to atoms. *New J. Phys.* **12**, 083053 (2010). doi: 10.1088/1367-2630/12/8/083053
51. F. Calegari *et al*., Charge migration induced by attosecond pulses in bio-relevant molecules. *J. Phys. B At. Mol. Opt. Phys.* **49**, 142001 (2016). doi: 10.1088/0953-4075/49/14/142001
52. G. Hermann *et al*., Attosecond angular flux of partial charges on the carbon atoms of benzene in non-aromatic excited state. *Chem. Phys. Lett.* **683**, 553–558 (2017). doi: 10.1016/j.cplett.2017.01.030
53. R. M. Kerber, J. M. Fitzgerald, S. S. Oh, D. E. Reiter, O. Hess, Orbital angular momentum dichroism in nanoantennas. *Commun. Phys.* **1**, 87 (2018). doi: 10.1038/s42005-018-0088-2
54. See supplementary materials.
55. C. Hernández-García *et al*., High-order harmonic propagation in gases within the discrete dipole approximation. *Phys. Rev. A* **82**, 033432 (2010). doi: 10.1103/PhysRevA.82.033432
56. C. Hernández-García *et al*., Extreme ultraviolet vector beams driven by infrared lasers. *Optica* **4**, 520 (2017). doi: 10.1364/OPTICA.4.000520
57. M. Lewenstein, P. Balcou, M. Y. Ivanov, A. L'Huillier, P. B. Corkum, Theory of high-harmonic generation by low-frequency laser fields. *Phys. Rev. A* **49**, 2117–2132 (1994). doi: 10.1103/PhysRevA.49.2117; pmid: 9910464
58. A. Zaïr *et al*., Quantum path interferences in high-order harmonic generation. *Phys. Rev. Lett.* **100**, 143902 (2008). doi: 10.1103/PhysRevLett.100.143902; pmid: 18518033
59. M. V. Berry, Optical vortices evolving from helicoidal integer and fractional phase steps. *J. Opt. A, Pure Appl. Opt.* **6**, 259–268 (2004). doi: 10.1088/1464-4258/6/2/018
60. J. Leach, E. Yao, M. Padgett, Observation of the vortex structure of non-integer vortex beam. *New J. Phys.* **6**, 71 (2004). doi: 10.1088/1367-2630/6/1/071
61. S. N. Alperin, M. E. Siemens, Angular Momentum of Topologically Structured Darkness. *Phys. Rev. Lett.* **119**, 203902 (2017). doi: 10.1103/PhysRevLett.119.203902; pmid: 29219346
62. E. Karimi, L. Marrucci, C. de Lisio, E. Santamato, Time-division multiplexing of the orbital angular momentum of light. *Opt. Lett.* **37**, 127–129 (2012). doi: 10.1364/OL.37.000127; pmid: 22854442
63. I. J. Sola *et al*., Controlling attosecond electron dynamics by phase-stabilized polarization gating. *Nat. Phys.* **2**, 319–322 (2006). doi: 10.1038/nphys281
64. H. Vincenti, F. Quéré, Attosecond lighthouses: How to use spatiotemporally coupled light fields to generate isolated attosecond pulses. *Phys. Rev. Lett.* **108**, 113904 (2012). doi: 10.1103/PhysRevLett.108.113904; pmid: 22540475
65. J. A. Wheeler *et al*., Attosecond lighthouses from plasma mirrors. *Nat. Photonics* **6**, 829–833 (2012). doi: 10.1038/nphoton.2012.284
66. C. Hernández-García, A. Jaron-Becker, D. D. Hickstein, A. Becker, C. G. Durfee, High-order-harmonic generation driven by pulses with angular spatial chirp. *Phys. Rev. A (Coll. Park)* **93**, 023825 (2016). doi: 10.1103/PhysRevA.93.023825
67. I. P. Christov, M. M. Murnane, H. C. Kapteyn, High-harmonic generation of attosecond pulses in the "single cycle" regime. *Phys. Rev. Lett.* **78**, 1251–1254 (1997). doi: 10.1103/PhysRevLett.78.1251
68. M. Chini, K. Zhao, Z. Chang, The generation, characterization and applications of broadband isolated attosecond pulses. *Nat. Photonics* **8**, 178–186 (2014). doi: 10.1038/nphoton.2013.362
69. W. Holgado *et al*., Continuous spectra in high-harmonic generation driven by multicycle laser pulses. *Phys. Rev. A* **93**, 013816 (2016). doi: 10.1103/PhysRevA.93.013816
70. J. Zhang, S.-J. Huang, F.-Q. Zhu, W. Shao, M.-S. Chen, Dimensional properties of Laguerre-Gaussian vortex beams. *Appl. Opt.* **56**, 3556–3561 (2017). doi: 10.1364/AO.56.003556; pmid: 28430234
71. Y. Esashi *et al*., Ptychographic amplitude and phase reconstruction of bichromatic vortex beams. *Opt. Express* **26**, 34007–34015 (2018). doi: 10.1364/OE.26.034007; pmid: 30650831

ACKNOWLEDGMENTS

Funding: C.H.-G., J.S.R., and L.P. acknowledge support from Junta de Castilla y León (SA046U16), Ministerio de Economía y Competitividad (FIS2016-75652-P), FEDER funds, and Ministerio de Ciencia, Innovación y Universidades (Eq. C2018-0041 17-P). L.R. acknowledges support from Ministerio de Educación, Cultura y Deporte (FPU16/02591). C.H.-G. acknowledges support from a 2017 Leonardo Grant for Researchers and Cultural Creators, BBVA Foundation, and Ministerio de Ciencia, Innovación y Universidades for a Ramón y Cajal contract (RYC-2017-22745), cofunded by the European Social Fund. H.K. and M.M. acknowledge support from the Department of Energy BES Award no. DE-FG02-99ER14982 for the experimental implementation, the DARPA TEE Program Award. no. D18AC00017 for the new experimental characterization methods developed, as well as a MURI grant from the Air Force Office of Scientific Research under Award no. FA9550-16-1-0121 for the theory. Q.L.N. acknowledges support from National Science Foundation Graduate Research Fellowships (grant no. DGE-1144083). N.J.B. and D.C. acknowledge support from National Science Foundation Graduate Research Fellowships (grant no. DGE-1650115). E.P. acknowledges Cellex-ICFO-MPQ fellowship funding; E.P. and M.L. acknowledge the Spanish Ministry MINECO (National Plan 15 Grant: FISICATEAMO no. FIS2016-79508-P, SEVERO OCHOA no. SEV-2015-0522, FPI), European Social Fund, Fundació Cellex, Generalitat de Catalunya (AGAUR grant no. 2017 SGR 1341 and CERCA/Program), ERC AdG OSYRIS, EU FETPRO QUIC, and the National Science Centre, Poland-Symfonia grant no. 2016/20/W/ST4/00314. We acknowledge the computer resources at MareNostrum and the technical support provided by Barcelona Supercomputing Center (RES-AECT-2014-2-0085). This research made use of the high-performance computing resources of the Castilla y León Supercomputing Center (SCAYLE, www.scayle.es/), financed by the European Regional Development Fund (ERDF). **Author contributions:** L.R., J.S.R, L.P., and C.H.-G. conceived the idea of self-torqued beams. K.M.D., L.R., H.C.K., M.M.M., and C.H.-G. designed the experiment. K.M.D., N.J.B., Q.L.N., C.-T.L., D.E.C., and A.L. conducted the experiment. K.M.D. and N.J.B. analyzed the experimental data. L.R., J.S.R., L.P., E.P., and C.H.-G. performed the theoretical simulations and analyzed the resulting data. C.H.-G., L.P., M.L., M.M.M., and H.C.K. supervised the theoretical simulations, experimental work, and developed the facilities and measurement capabilities. L.R., K.M.D., J.S.R., M.M.M., L.P., and C.H.-G. wrote and prepared the manuscript. All authors provided constructive improvements and feedback to this work. **Competing interests:** M.M.M. and H.C.K. have a financial interest in KMLabs. All other authors declare no competing financial interests. **Data and materials availability:** All data needed to evaluate the conclusions in the paper are present in the paper or the supplementary materials.

SUPPLEMENTARY MATERIALS

science.sciencemag.org/content/364/6447/eaaw9486/suppl/DC1
Supplementary Text
Figs. S1 to S8
References (*72*–*79*)
Movie S1

8 February 2019; accepted 3 May 2019
10.1126/science.aaw9486

Generation of extreme-ultraviolet beams with time-varying orbital angular momentum

Laura Rego, Kevin M. Dorney, Nathan J. Brooks, Quynh L. Nguyen, Chen-Ting Liao, Julio San Román, David E. Couch, Allison Liu, Emilio Pisanty, Maciej Lewenstein, Luis Plaja, Henry C. Kapteyn, Margaret M. Murnane and Carlos Hernández-García

Science **364** (6447), eaaw9486.
DOI: 10.1126/science.aaw9486

Pulses with a twist and torque

Structured light beams can serve as vortex beams carrying optical angular momentum and have been used to enhance optical communications and imaging. Rego *et al.* generated dynamic vortex pulses by interfering two incident time-delayed vortex beams with different orbital angular momenta through the process of high harmonic generation. A controlled time delay between the pulses allowed the high harmonic extreme-ultraviolet vortex beam to exhibit a time-dependent angular momentum, called self-torque. Such dynamic vortex pulses could potentially be used to manipulate nanostructures and atoms on ultrafast time scales.

Science, this issue p. eaaw9486